

# Restoring Coherence Lost to a Mesoscopic Bath

Wang Yao<sup>1</sup>, Ren-Bao Liu<sup>1†</sup> & L. J. Sham<sup>1</sup>

<sup>1</sup>*Department of Physics, University of California San Diego, La Jolla, California 92093-0319, USA*

†Present address: Department of Physics, The Chinese University of Hong Kong, Hong Kong, China

**A quantum system, unlike a classical one, can be in a coherent superposition of constituent states. This coherence is the wellspring of quantum properties and key to quantum technology. The contact of a quantum object with a macroscopic system causes loss of state coherence<sup>1</sup>. Advances towards quantum technology have effectively substituted the macroscopic environments by mesoscopic ones. The coupled dynamics of the quantum object and the mesoscopic bath, within timescales of interest, is treated here as a coherent quantum evolution of an isolated system, where the decoherence of the quantum object results from the entanglement with the bath established by this evolution<sup>2,3,4,5</sup>. We find that the mesoscopic bath dynamics is well described by a simple pseudo-spin model for the particle pair interaction in the bath, which leads to a theory of coherence recovery of the quantum object by disentanglement, realized through maneuvering the bath evolution by control of the quantum object. We apply such a quantum theory of decoherence control to one electron spin in a bath of many nuclear spins in a semiconductor quantum dot, a paradigmatic system in mesoscopic physics<sup>6,7</sup> and in spin-based quantum technology<sup>8,9,10</sup>.**

To show the quantum mechanics of decoherence<sup>2,3,4</sup>, we consider the simplest quantum object capable of only two possible states. We take the initial state to be a *prepared* micro-state  $|\phi^s(0)\rangle$ , which together with the bath state at that instant forms a single-product, or *unentangled* state,  $|\Psi(0)\rangle = |\phi^s(0)\rangle \otimes |J\rangle$ . Without loss of generality,

we use the spin language to depict the two-state object. Thus, the object, or spin, is in a coherent superposition of the spin up and down states  $|\pm\rangle$  in an external magnetic field,  $|\phi^s(0)\rangle = C_+|+\rangle + C_-|-\rangle$ . The state of the total system of the spin plus environment evolves over time  $t$  to  $|\Psi(t)\rangle = C_+(t)|+\rangle \otimes |J^+(t)\rangle + C_-(t)|-\rangle \otimes |J^-(t)\rangle$

which is *entangled*, i.e., no longer a single-product state when the environment states  $|J^\pm(t)\rangle$  are not the same. Physical observables of the quantum object is determined by

its reduced density matrix obtained by tracing over the environment states  $\rho_{\sigma,\sigma'}^s(t) = C_{\sigma'}^*(t)C_\sigma(t)\langle J^{\sigma'}(t)|J^\sigma(t)\rangle$ . The diagonal element of the reduced density matrix  $\rho_{\sigma,\sigma}^s$  gives the probability of finding the spin in state  $|\sigma\rangle$ . Either off-diagonal element is a measure of the coherence of the quantum object. The environment-driven shifting of the probability between the spin states is known as longitudinal relaxation. For application in quantum technology, the longitudinal relaxation can be virtually suppressed by setting the eigenenergy splitting of the spin to be much larger than the dominant excitation energies in the environment and the object-environment coupling strength<sup>11,12,13</sup>. Key to a quantum object being useful for quantum information processing is the prevention of pure dephasing (the decoherence in absence of longitudinal relaxation). When the cause of spin flip is removed, the reduced Hamiltonian of the whole system is in the form diagonal in quantum-object basis,  $\hat{H} = |+\rangle\langle+| \otimes \hat{H}^+ + |-\rangle\langle-| \otimes \hat{H}^-$ . The environment evolves under the Hamiltonian  $\hat{H}^\pm$  into separate pathways  $|J^\pm(t)\rangle \equiv e^{-i\hat{H}^\pm t}|J\rangle$  in the Hilbert space, depending on the quantum-object states. The pure dephasing is then measured by  $L_{+,-}^s(t) = |\langle J|e^{i\hat{H}^-t}e^{-i\hat{H}^+t}|J\rangle|$ . The above process can also be viewed as a measurement of the quantum object by the environment in which  $|J^\pm(t)\rangle$  act as two pointers and, as a consequence, the measured object will possess no coherence between the constituent states of the measurement basis<sup>14</sup>. A theory to ameliorate the pure dephasing is the objective of this paper. The coherence is restored by maneuvering the environment

dynamics with control of the quantum object so that the bifurcated pathways intersect at a later time, i.e.,  $|J^+(t)\rangle = |J^-(t)\rangle$ , leading to quantum disentanglement.

The coupled system of a quantum object and its environment is taken to be a spin 1/2 particle in a magnetic field and a mesoscopic bath of  $N$  mutually interacting spins that are in direct contact with the quantum object<sup>15</sup>. The isolation of the quantum object plus the meso-bath, in the relevant timescale, from the rest of universe arises out of their weak coupling with the outside. A specific example is a semiconductor quantum dot containing one electron spin and many nuclear spins. The spin bath is of broader scope since a  $j$ -spin may be mapped to a particle of  $2j+1$  energy levels. The orbital wave function of the quantum object covers all  $N$  bath spins (Fig. 1(b)) so that the interaction energy between the quantum object and each bath spin is  $\sim A/N$ , inversely proportional to the bath size  $N$ . The main assumption is the descending order of parameters with orders of magnitude differences,  $\Omega \gg \omega_n \gg A/N \gg b$ , where  $\omega_n$  characterizes the typical energy spacing of a bath spin and  $b$  the “short-range” direct interaction (referred here to those decaying no slower than dipolar) between two bath spins. Such a choice of system parameters is both feasible and required for the premise of a much longer longitudinal relaxation time of the quantum object than its pure dephasing time.

The form of the coupling between the quantum-object spin  $\hat{\mathbf{S}}$  and the bath spin  $\hat{\mathbf{J}}_n, n=1, \dots, N$  is a linear combination of  $\hat{S}^\alpha \hat{J}_n^\alpha$  of the Cartesian components  $\alpha = x, y, z$ . By convention,  $\hat{S}^z$  along the magnetic field yields the energy splitting  $\Omega$  and its coupling to the environment observables  $\hat{J}_n^z$  is the longitudinal coupling. The transverse coupling is of the flip-flop form  $\hat{S}^\pm \hat{J}_n^\mp$  where  $\hat{S}^\pm = \hat{S}^x \pm i\hat{S}^y$  and similar for  $\hat{J}_n^\pm$ . We remove the contribution of this transverse coupling to longitudinal relaxation by a canonical transformation but keep the resultant second order effective interaction between two bath spins mediated by virtue flips of the quantum-object spin (see the

Supplementary Information and Ref. 16). This mediated interaction ( $\sim A^2/(N^2\Omega)$ ) couples any two spins in the meso-bath and is differentiated from the “short-range” interaction above by the qualifier “infinite-range”. Its dependence on the number of particles in the bath suggests its mesoscopic nature. The resultant Hamiltonian for the system is of the reduced form discussed above, diagonal in the quantum-object states  $|\pm\rangle$ .

The mesoscopic nature is essential in our theory from the conditions  $N^2b^2A^{-2} \ll 1 \ll \min(\sqrt{N}, N^4b^2\Omega^4A^{-6})$  to be established below (see also the Supplemental Information for details). The upper bound for  $N$  distinguishes the bath from a macroscopic system whose bulk properties per particle are independent of  $N$ . It leads to the dominance of the pair correlation in the interaction dynamics, due to short-range direct interactions, of the bath spins over the correlations of more than two particles. The lower bound,  $N^4b^2\Omega^4A^{-6} \gg 1$ , is by a similar consideration but due to the infinite-range mediated interaction of the bath spins. The lower bound  $\sqrt{N} \gg 1$  simply signifies the necessary statistics for decoherence. In the case of the electron spin in a GaAs quantum dot, the theory is well justified for  $10^8 \geq N \geq 10^4$  which covers quantum dots of all practical sizes.

The meso-bath dynamics is well described by a pseudo-spin model. The interaction between two bath spins labelled  $(n,m)$  excites one and de-excites the other, from state  $|j_n\rangle|j_m\rangle$  to state  $|j_n+1\rangle|j_m-1\rangle$ , where  $j$  is the quantum number for the  $z$ -component of bath spin. Each pair-flip process of the above form, indexed by  $k$ , is characterized by the energy cost  $\pm E_k + D_k$  and the transition matrix element  $\pm A_k + B_k$  depending on the quantum object state  $|\pm\rangle$ .  $\pm E_k$  ( $\sim A/N$ ) is from the longitudinal object-bath interaction,  $D_k$  ( $\sim b$ ) and  $B_k$  ( $\sim b$ ) are, respectively, due to the longitudinal and transverse part of the short-range direct interactions between bath spins, and  $A_k$  ( $\sim A^2/N^2\Omega$ ) is the infinite-range bath spin interaction mediated by the quantum

object.  $A_k$  dominates the dynamics of non-local (widely separated) bath spin pairs while the  $B_k$  is typically more important for local pair dynamics.  $D_k \ll E_k$  under the mesoscopic condition above. We map the two pair states  $|j_n\rangle|j_m\rangle$  and  $|j_n+1\rangle|j_m-1\rangle$  respectively into the eigenstates of a pseudo-spin 1/2:  $|\uparrow\rangle_k$  and  $|\downarrow\rangle_k$ . The bath is driven by the effective Hamiltonian

$$\hat{H}^\pm \cong \sum_k \hat{H}_k^\pm = \sum_k \mathbf{h}_k^\pm \cdot \hat{\boldsymbol{\sigma}}_k / 2, \quad (1)$$

where  $\hat{\boldsymbol{\sigma}}_k$  are the Pauli matrices. Each pseudo-spin is driven by the effective magnetic field  $\mathbf{h}_k^\pm \equiv (2B_k \pm 2A_k, 0, D_k \pm E_k)$  depending on the state of the quantum object,  $|\pm\rangle$ .

The pseudo-spin model is an approximation including only pair correlations<sup>16,17</sup> (see the Supplemental Information). The quantum-object decoherence due to local and non-local bath spin pair dynamics has different dependence on the bath size because of the different  $N$ -dependence of  $A_k, B_k$  and the different numbers of local and non-local pairs. The short-range direct interaction dominates the large  $N$  end of the mesoscopic regime while the infinite-range mediated interaction dominates the small  $N$  end<sup>16</sup>.

We consider first the decoherence due to the quantum fluctuation from a pure state of the bath and then the thermal fluctuations of an ensemble of bath states. A natural basis set for the bath is the product states  $|J\rangle \equiv \bigotimes_n |j_n\rangle$  which are eigenstates of all the spin components along the magnetic field<sup>18</sup>. The bath is assumed of high entropy (i.e., the temperature is high for the bath spins). This condition, together with the lower bound  $\sqrt{N} \gg 1$ , ensures a sufficiently large number of decoherence channels in the bath for the quantum evolution to be a real irreversible dynamics (the period of a Poincaré cycle is effectively infinite). The randomly chosen initial bath state  $|J\rangle$  is replaced by a product of independent states of pseudo-spins,  $\bigotimes_k |\uparrow\rangle_k$ , which represent all possible pair combinations of the particle states. The dynamics of each possible pair state from the initial state  $|J\rangle$  is explicitly described as precession of an independent pseudo-spin

initially along the pseudo  $+z$  axis under an effective magnetic field  $\mathbf{h}_k^\pm$  depending on the  $|\pm\rangle$  state of the quantum object. Thus, the spin coherence is  $L_{+,-}^s(t) \equiv \prod_k \left| \langle \psi_k^- | \psi_k^+ \rangle \right|$  where  $|\psi_k^\pm\rangle = e^{-i\mathbf{h}_k^\pm \cdot \hat{\sigma}_k t/2} |\uparrow\rangle_k$  are the conjugate pseudo-spin states evolving from the same initial state  $|\uparrow\rangle_k$ .

The simple, conditional form of the pseudo-spin (or pair-state) evolution enables us to study possible shepherding of the meso-bath state by controlling the quantum object. To be specific, we consider from now on the problem of a single electron spin in a GaAs quantum dot. A short  $\pi$ -rotation pulse applied at  $t = \tau$  to flip the electron spin<sup>19</sup> would cause the pseudo-spin evolution

$$|\psi_k^\pm\rangle = e^{-i\mathbf{h}_k^\mp \cdot \hat{\sigma}_k (t-\tau)/2} e^{-i\mathbf{h}_k^\pm \cdot \hat{\sigma}_k \tau/2} |\uparrow\rangle_k. \quad (2)$$

The quantum evolution of the non-local bath spin pairs is almost completely reversed under the influence of the electron spin flip due to the symmetry of the dominant part of the effective field  $\mathbf{h}_k^\pm \equiv \pm(2A_k, 0, E_k)$ . Disentanglement of the electron spin from non-local bath spin pairs is obvious at  $2\tau$ . Evolution of local bath spin pairs lacks this time reversal symmetry (the dominant part of the effective magnetic field is  $\mathbf{h}_k^\pm \equiv (2B_k, 0, \pm E_k)$  instead), and has non-trivial trajectories under the influence of the electron spin flip. Disentanglement from all local pairs and, hence, a recovery of the electron spin coherence occurs at time  $\sqrt{2}\tau$ . This is illustrated by a numerical evaluation for the electron spin in a dot of  $10^6$  nuclear spins which reveals the coherence revival after a flip of the electron spin at various  $\tau$ , even when the coherence has visibly vanished (see Fig. 1(c,d)). In this pure state dynamics, the electron spin decoherence results solely from the quantum evolution induced object-bath entanglement and the coherence restoration is a consequence of the disentanglement of the quantum object and the bath. The disentanglement is in stark contrast to the classical

phase refocusing (spin echo) of an ensemble of spins with inhomogeneous broadening<sup>20</sup>, as unambiguously evidenced by the fact that the spin echo occurs at  $2\tau$  instead of  $\sqrt{2}\tau$ .

The disentanglement and, hence, the restoration of lost coherence can be understood in a geometrical picture based on the pseudo-spin rotation. The quantum evolution of the pseudo-spins conditioned on the electron spin states  $|\pm\rangle$  is described by two conjugate Bloch vectors,  $\langle\psi_k^\pm|\hat{\sigma}_k/2|\psi_k^\pm\rangle$ , precessing about their respective effective magnetic fields  $\mathbf{h}_k^\pm$ . The entanglement between the electron spin and the pseudo spin is measured by the distance  $\delta_k$  between the conjugate vectors which is related to the state overlap by  $\delta_k^2 = 1 - \left|\langle\psi_k^-|\psi_k^+\rangle\right|^2$ . Thus, the electron spin coherence is given by

$$L_{+,-}^s(t) = \prod_k \sqrt{1 - \delta_k^2} \cong \exp\left(-\sum_k \delta_k^2/2\right), \quad (3)$$

where the approximation holds for  $|\delta_k| \ll 1$  as a result of  $t \ll B_k^{-1}, A_k^{-1}$ . We focus below on the non-trivial local pair dynamics of bath spins. In Fig. 1(e,f), the electron spin decoherence is clearly illustrated by the initial increase of the distance  $\delta_k$ . The route to disentanglement between the electron and the nuclear bath is now transparent: upon a controlled  $\pi$ -flip of the electron spin, the conjugate Bloch vectors exchange their effective magnetic fields ( $\mathbf{h}_k^+ \leftrightarrow \mathbf{h}_k^-$ ), causing their subsequent trajectories to intersect. Even though different pseudo spins can have different precession frequencies  $h_k \equiv \sqrt{E_k^2 + 4B_k^2}$ , the distance  $\delta_k$  is eliminated for all pseudo spins in the leading order of  $bt$  at  $t = \sqrt{2}\tau$  as

$$\delta_k^2 = E_k^2 B_k^2 \left(t^2 - 2\tau^2\right)^2 + O\left(E_k^2 B_k^2 D_k^2 \tau^6\right). \quad (4)$$

Compared to the free-induction decay where  $\delta_k^2 \sim E_k^2 B_k^2 t^4$  for local pair-flips<sup>16</sup>, the decoherence is reduced at the disentanglement point by a factor of  $\sim D_k^2 \tau^2$  ( $\sim 10^{-4}$  for

$\tau \sim 10\mu\text{s}$ ). Similar to the single-pulse control, the coherence may be restored by a sequence of  $\pi$ -rotations of the electron spin. For example, with a sequence of  $\pi$ -pulses evenly spaced with interval  $\tau$ , the disentanglement from the bath will occur, with residue  $\delta_k^2 \sim E_k^2 B_k^2 D_k^2 \tau^6$ , at every  $\sqrt{n(n+1)}\tau$  between the  $n$ th and the  $(n+1)$ th pulses, as illustrated in Fig. 1(g).

In the pure state dynamics, the evolution of the quantum object is also affected by a bath configuration dependent field resulted from its longitudinal coupling to the bath spins, i.e., in the case of the electron spin in quantum dot, the nuclear Overhauser field. Denoting its spin splitting in the Overhauser field of  $|J\rangle$  as  $E_J$ , the complete description to the quantum object coherence is  $\rho_{+-}(t) = C_-^* C_+ e^{-i\phi_J(t)} L_{+-}^s(t)$  where the phase  $\phi_J(t) = E_J \left[ \tau_1 - (\tau_2 - \tau_1) + \dots + (-1)^n (\tau_n - \tau_1) \right]$  under the control of a sequence of  $\pi$ -rotations on quantum object at  $\tau_1, \tau_2, \dots$ , and  $\tau_n$  respectively. The  $L_{+-}^s(t)$  part is, however, insensitive, up to a factor of  $1/\sqrt{N} \ll 1$ , to the selection of initial bath state  $|J\rangle \equiv \bigotimes_n |j_n\rangle$ , verified by numerical evaluations on bath states associated with different Overhauser fields<sup>16</sup>.

The coherence restoration at the unusual time  $t = \sqrt{n(n+1)}\tau$  is observable in principle in single spin measurement with pre-determination or post-selection of bath Overhauser field through projective measurement<sup>18</sup>, but it could be concealed by inhomogeneous broadening in ensemble measurements<sup>19,21,22,23</sup>. The ensemble-averaged coherence of the quantum object can be expressed as  $\rho_{+-}(t) = C_-^* C_+ L_{+-}^s(t) \times L_{+-}^0(t)$ , where  $L_{+-}^0(t) \equiv \sum_J p_J e^{-i\phi_J(t)}$  is the inhomogeneous broadening factor due to the distribution of the Overhauser field and  $p_J$  is the probability of having the bath configuration  $|J\rangle$ , e.g., in the thermal ensemble. With a sequence of  $\pi$ -rotations on the quantum object,  $L_{+-}^0(t)$  can be stroboscopically restored to unity at each spin-echo time  $t$  fulfilling the phase refocusing condition  $\tau_1 - (\tau_2 - \tau_1) + \dots + (-1)^n (\tau_n - \tau_1) = 0$  with the width of each echo given by the ensemble dephasing time  $T_2^*$ <sup>19,21</sup>. Since  $T_2^*$  ( $\sim 1-10\text{ ns}$

in GaAs dots<sup>21,22,23</sup>) is much shorter than the decoherence time determined by the quantum entanglement in the pure state dynamics (denoted by  $T_2$ ,  $\sim 10\mu\text{s}$  from Fig.1), the inhomogeneous dephasing  $L_{+,-}^0(t)$  will virtually conceal the rich features of  $L_{+,-}^s(t)$ , except for those coinciding with the classical phase refocusing.

To observe coherence restoration in ensemble experiments, the time for quantum disentanglement has to coincide with that of spin echo. The disentanglement from non-local bath pairs always coincides with the classical phase refocusing. The non-trivial job is to design a pulse sequence so that disentanglement from all local bath pairs occurs at the spin-echo time as well. The simplest solution is a two-pulse sequence. The geometrical picture of the local pair evolution (see Fig. 2(a)) shows that a second  $\pi$ -rotation of quantum object makes the conjugate vectors of a pseudo-spin meet again. This secondary disentanglement can indeed coincide with the secondary spin echo if the timing of the two pulses satisfies  $\tau_2/3 = \tau_1 \equiv \tau$ , amounting to the famous Carr-Purcell pulse sequence in NMR spectroscopies<sup>20</sup>. The residue  $\delta_k^2$  at  $t = 4\tau$  under this two pulse control is

$$\delta_k^2(4\tau) = 16(E_k B_k - A_k D_k)^2 D_k^2 \tau^6, \quad (5)$$

where the leading order contribution to the decoherence has been successfully eliminated. The restoration of coherence in ensemble dynamics by the two-pulse control is clearly demonstrated by numerical evaluation as shown in Fig 2(b,c). Remarkably, the electron spin coherence can be largely restored at  $4\tau$  by the second  $\pi$ -pulse even when the first spin-echo at  $2\tau$  has completely vanished. Note that the absence of spin echo does not mean irreversible loss of coherence<sup>24</sup>.

The pseudo-spin evolution with the two-pulse control of the quantum object can be constructed recursively from the free-induction evolution as  $\hat{U}_0^\pm = e^{-i\mathbf{h}_k^\pm \cdot \hat{\sigma}_k \tau/2}$ ,  $\hat{U}_1^\pm = \hat{U}_0^\mp \hat{U}_0^\pm$  and  $\hat{U}_2^\pm = \hat{U}_1^\mp \hat{U}_1^\pm$ . This observation indicates a pulse sequence design

strategy by concatenation as recently adopted in the context of dynamical decoupling in quantum computation<sup>25</sup>. The pseudo-spin evolution under the concatenated control is constructed by iteration (see Fig. 2(d))

$$\hat{U}_l^{\pm} = \hat{U}_{l-1}^{\mp} \hat{U}_{l-1}^{\pm} \equiv e^{-i\theta_{l-1}^{\pm} \cdot \hat{\sigma}_k / 2}, \quad (6)$$

and a disentanglement will occur at  $\tau_l = 2^l \tau$  coinciding with a spin echo. Here we have introduced the vector rotation angle  $\theta_l^{\pm}$  for a pictorial understanding of the concatenation control (see Fig. 2(e)). When the rotation angle  $\theta_l^{\pm}$  is small, its recursion has a simple geometrical representation

$$\theta_{l+1}^{\pm} = \theta_l^+ + \theta_l^- \mp \theta_l^+ \times \theta_l^-. \quad (7)$$

By each level of iteration, the vector rotation angles for the conjugate pseudo-spins has the common part  $(\theta_l^+ + \theta_l^-)/2$  increased by a factor of 2 and the difference  $(\theta_l^+ - \theta_l^-)$  reduced by a factor of  $\theta_l^{\pm}$  ( $\sim 2^l b\tau$  by noting that the free-induction evolution  $\theta_0^{\pm} \sim b\tau$ ). The decoherence is reduced by an order of  $2^{2l} b^2 \tau^2$  at  $\tau_l$  for each additional level of concatenation until saturated at the level  $l_0 = -\log_2(b\tau)$ . Hence, the coherence echo magnitude scales with the echo delay time according to  $\exp(-(\tau_l / T_l)^n)$ ,  $n = 2(l+1)$  as shown in Fig. 2(f).

The pulse sequence design is borrowed from the dynamical decoupling schemes in NMR spectroscopies<sup>20</sup> and in quantum computation<sup>25,26,27</sup>, but the disentanglement method aims directly at the bath dynamics. It does not seek to cancel the object-bath interaction by dynamical averaging, but instead, with the solution of mesoscopic bath dynamics, implements coherence control by maneuvering the bath evolution. In general, elimination of object-bath coupling is not a necessary condition for their disentanglement. For instance, at disentanglement time  $\sqrt{2}\tau$  by the single pulse control, the effective object-bath interaction  $\hat{S}^z \otimes \hat{H}_{\text{eff}}$ , defined by  $\hat{H}_{\text{eff}} \equiv \hat{H}_{\text{eff}}^+ - \hat{H}_{\text{eff}}^-$  where

$e^{-i\hat{H}_{\text{eff}}^{\pm}\sqrt{2}\tau} \equiv e^{-i\hat{H}^{\mp}(\sqrt{2}-1)\tau}e^{-i\hat{H}^{\pm}\tau}$ , does not vanish even in the first order of the object-bath coupling ( $A/N$ ). As demonstrated in Fig. 1(g), the disentanglement times are not equally spaced even though the controlling pulses are. In the concatenated design of disentanglement sequence, the bath internal coupling strength  $b$ , rather than the object-bath coupling strength  $A/N$  as in dynamical decoupling<sup>27</sup>, acts as the controlling parameter in determining the leftover decoherence. Since  $b \ll A/N$  in the mesoscopic bath, the restriction on the interpulse interval  $\tau$  of control pulses is substantially relaxed. In the practical example of nuclear spin bath in quantum dot ( $(A/N)^{-1} \sim \mu\text{s}$ ,  $b^{-1} \sim \text{ms}$ ), our calculation shows that the electron spin coherence is well protected by pulse sequences with interpulse interval up to  $\sim 10 \mu\text{s}$ . Thus, the disentanglement scheme opens up another perspective to coherence protection in mesoscopic systems, complementary to the dynamical decoupling<sup>25,26,27</sup>, the quantum error correction<sup>28</sup> and the decoherence-free subspace method<sup>29,30,31</sup>.

1. Gardiner, C. W. & Zoller, P. *Quantum Noise* (Springer, Berlin, 2000).
2. Zurek, W. H. Decoherence, einselection, and the quantum origins of the classical. *Rev. Mod. Phys.* **75**, 715-775 (2003).
3. Joos, E., Zeh, H. D., Kiefer, C., Giulini, D., Kupsch, J. & Stamatescu, I. -O. *Decoherence and the appearance of a classical world in quantum theory* (Springer, New York, 2003).
4. Schlosshauer, M. Decoherence, the measurement problem, and interpretations of quantum mechanics. *Rev. Mod. Phys.* **76**, 1267-1305 (2004).
5. Buscemi, F., Chiribella, G. & D'Ariano, G. M. Inverting Quantum Decoherence by Classical Feedback from the Environment. *Phys. Rev. Lett.* **95**, 090501 (2005).
6. Leggett, A. J., Chakravarty, S., Dorsey, A. T., Fisher, M. P. A., Garg, A. & Zwerger, W. Dynamics of the dissipative 2-state system. *Rev. Mod. Phys.* **59**, 1-85 (1987).

7. Imry, Y. *Introduction to mesoscopic physics* (Oxford Univ. Press, New York, 1997).
8. Loss, D. & DiVincenzo, D. P. Quantum computation with quantum dots. *Phys. Rev. A* **57**, 120-126 (1998).
9. Awschalom, D. D., Loss, D. & Samarth, N. (eds). *Semiconductor spintronics and quantum computation* (Springer, New York, 2000).
10. Imamoglu, A., Awschalom, D. D., Burkard, G., DiVincenzo, D. P., Loss, D., Sherwin, M. & Small, A. Quantum Information Processing Using Quantum Dot Spins and Cavity QED. *Phys. Rev. Lett.* **83**, 4204-4207 (1999).
11. Fujisawa, T., Austing, D. G., Tokura, Y., Hirayama, Y. & Tarucha, S. Allowed andn forbidden transitions in artificial hydrogen and helium atoms. *Nature* **419**, 278-281 (2002).
12. Elzerman, J. M., Hanson, R., van Beveren, L. H. W., Witkamp, B., Vandersypen, L. M. K. & Kouwenhoven, L. P. Single-shot read-out of an individual electron spin in a quantum dot. *Nature* **430**, 431-435 (2004).
13. Kroutvar, M., Ducommun, Y., Heiss, D., Bichler, M., Schuh, D., Abstreiter, D. & Finley, J. J. Optically programmable electron spin memory using semiconductor quantum dots. *Nature* **432**, 81-84 (2004).
14. Brune, M., Hagley, E., Dreyer, J., Maitre, X., Maali, A., Wunderlich, C., Raimond, J. M. & Haroche, S. Observing the Progressive Decoherence of the “Meter” in a Quantum Measurement. *Phys. Rev. Lett.* **77**, 4887-4890 (1996)
15. Prokof'ev, N. V. & Stamp, P. C. E., Theory of the spin bath. *Rep. Prog. Phys.* **63**, 669-726 (2000).
16. Yao, W., Liu, R. B. & Sham, L. J. Theory of electron spin decoherence by interacting nuclear spins in a quantum dot. Preprint at (<http://arxiv.org/cond-mat/0508441>) (2005). Yao, W., Liu, R. B. & Sham, L. J. Unpublished data.

17. Witzel, W. M., de Sousa, R. & Das Sarma, S. Quantum theory of spectral diffusion induced electron spin decoherence. *Phys. Rev. B* **72**, 161306 (R) (2005).
18. Coish, W. A. & Loss, D. Hyperfine interaction in quantum dot: Non-markovian electron spin dynamics. *Phys. Rev. B* **70**, 195340 (2004).
19. Tyryshkin, A. M., Lyon, S. A., Astashkin, A. V. & Raitsimring, A. M. Electron spin relaxation times of phosphorus donors in silicon. *Phys. Rev. B* **68**, 193207 (2003).
20. Slichter, C. P. *Principles of Magnetic Resonance* (Springer-Verlag, New York, 1992).
21. Petta, J. R., Johnson, A. C., Taylor, J. M., Laird, E. A., Lukin, M. D., Marcus, C. M., Hanson, M. P. & Gossard, A. C. Coherent manipulation of coupled electron spins in semiconductor quantum dots. *Science* **309**, 2180-2184 (2005).
22. Koppens, F. H. L., Folk, J. A., Elzerman, J. M., Hanson, R., van Beveren, L. H. W., Vink, I. T., Tranitz, H. P., Wegscheider, W., Kouwenhoven, L. P., & Vandersypen, L. M. K. Control and detection of singlet-triplet mixing in a random nuclear field. *Science* **309**, 1346-1350 (2005).
23. Bracker, A. S., Stinaff, E. A., Gammon, D., Ware, M. E., Tischler, J. G., Shabaev, A., Efros, Al. L., Park, D., Gershoni, D., Korenev, V. L. & Merkulov., I. A. Optical pumping of the electronic and nuclear spin of single charge-tunable quantum dots. *Phys. Rev. Lett.* **94**, 047402 (2005).
24. Rhim, W. -K., Pines, A. & Waugh, J. S. Violation of the Spin-Temperature Hypothesis. *Phys. Rev. Lett.* **25**, 218-220 (1970).
25. Khodjasteh, K. & Lidar, D. A. Fault-tolerant quantum dynamical decoupling. *Phys. Rev. Lett.* **95**, 180501 (2005).
26. Viola, L., & Lloyd, S. Dynamical suppression of decoherence in two-state quantum systems. *Phys. Rev. A* **58**, 2733-2744 (1998).

27. Viola, L. & Knill, E. Random decoupling schemes for quantum dynamical control and error suppression. *Phys. Rev. Lett.* **94**, 060502 (2005).
28. Nielsen, M. A. & Chuang, I. L. *Quantum Computation and Quantum Information* (Cambridge University Press, Cambridge, 2000).
29. Duan, L. M. & Guo, G. C. Preserving coherence in quantum computation by pairing quantum bits. *Phys. Rev. Lett.* **79**, 1953-1956 (1997)
30. Lidar, D. A., Chuang, I. L. & Whaley, K. B. Decoherence-free subspaces for quantum computation. *Phys. Rev. Lett.* **81**, 2594-2597 (1998).
31. Zanardi, P. & Rasetti, M. Noiseless quantum codes. *Phys. Rev. Lett.* **79**, 3306-3309 (1997).

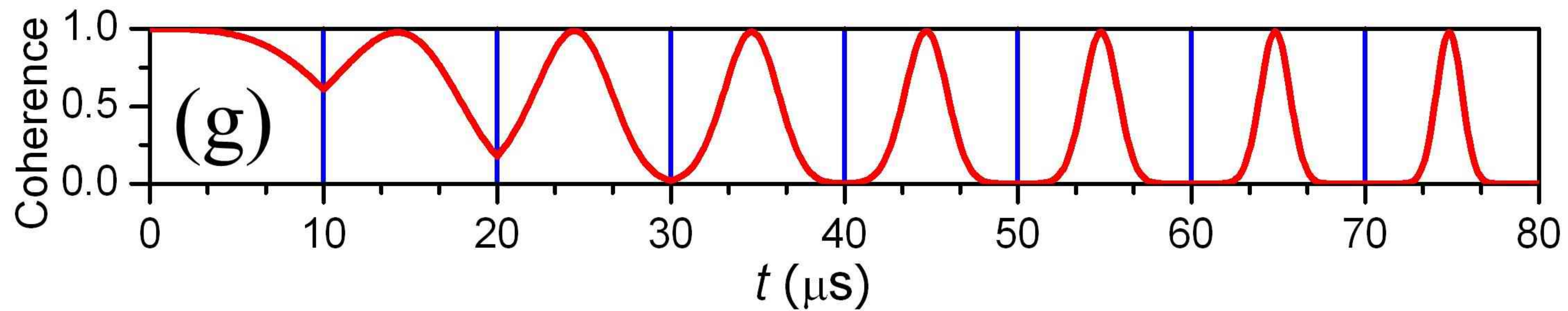
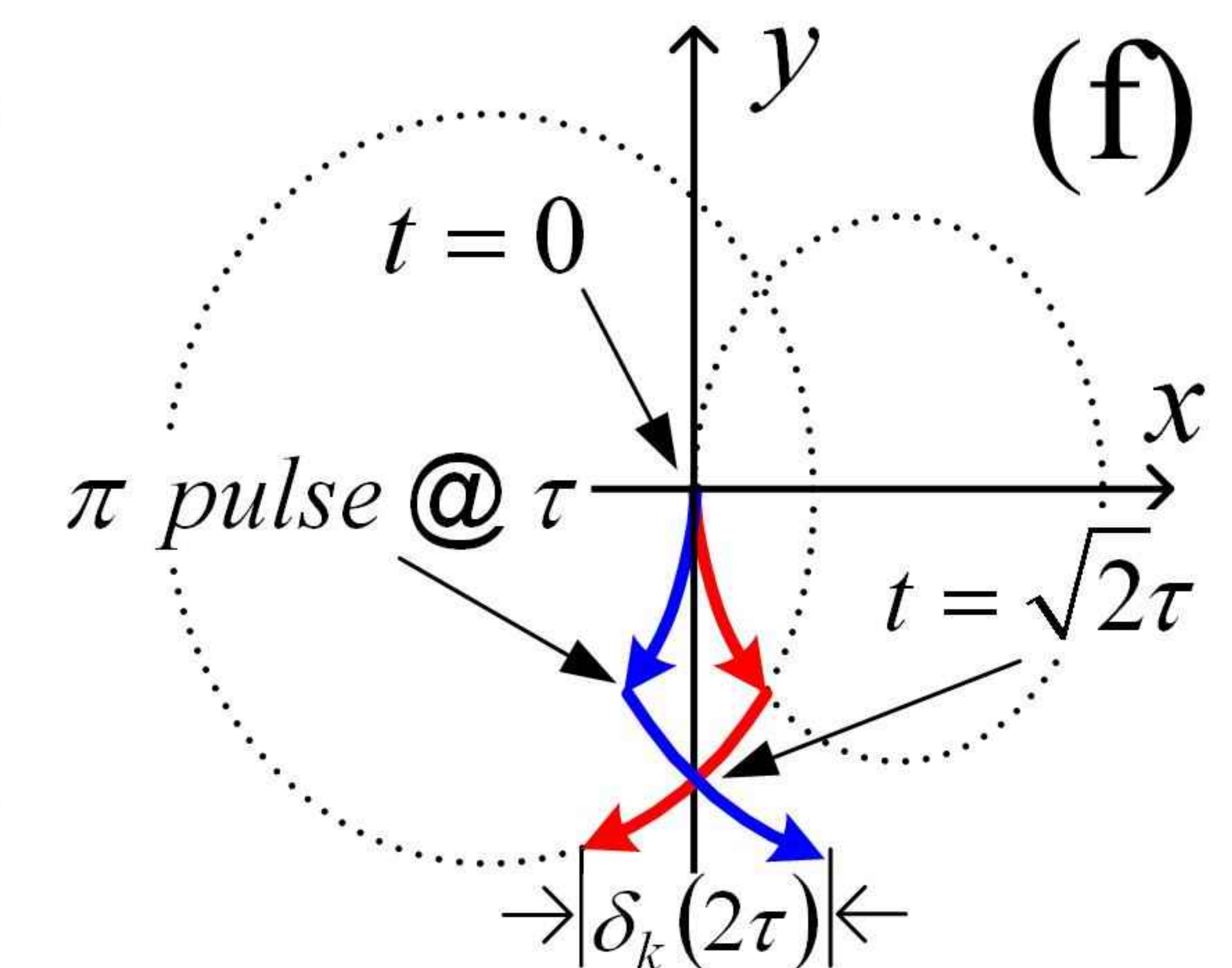
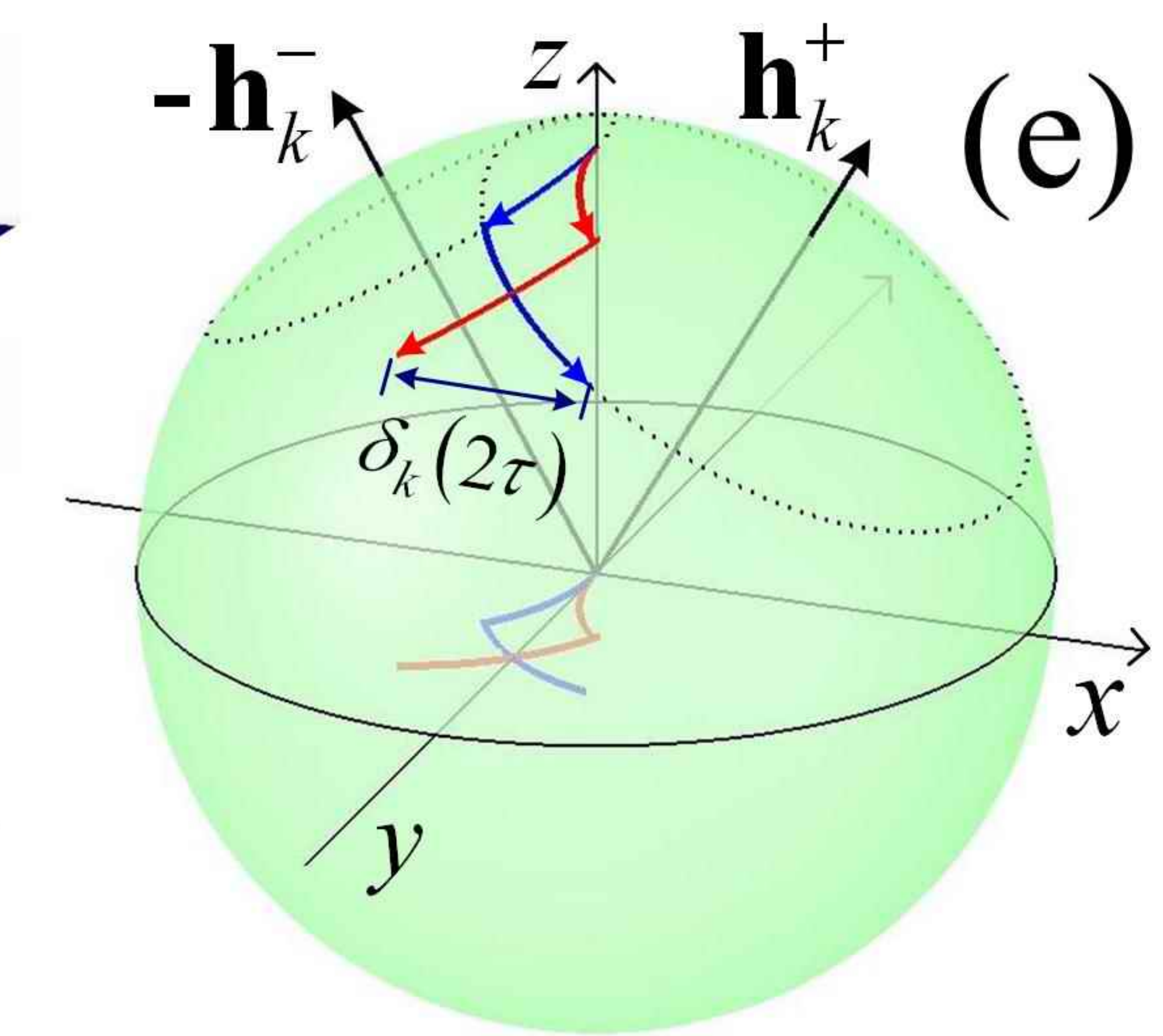
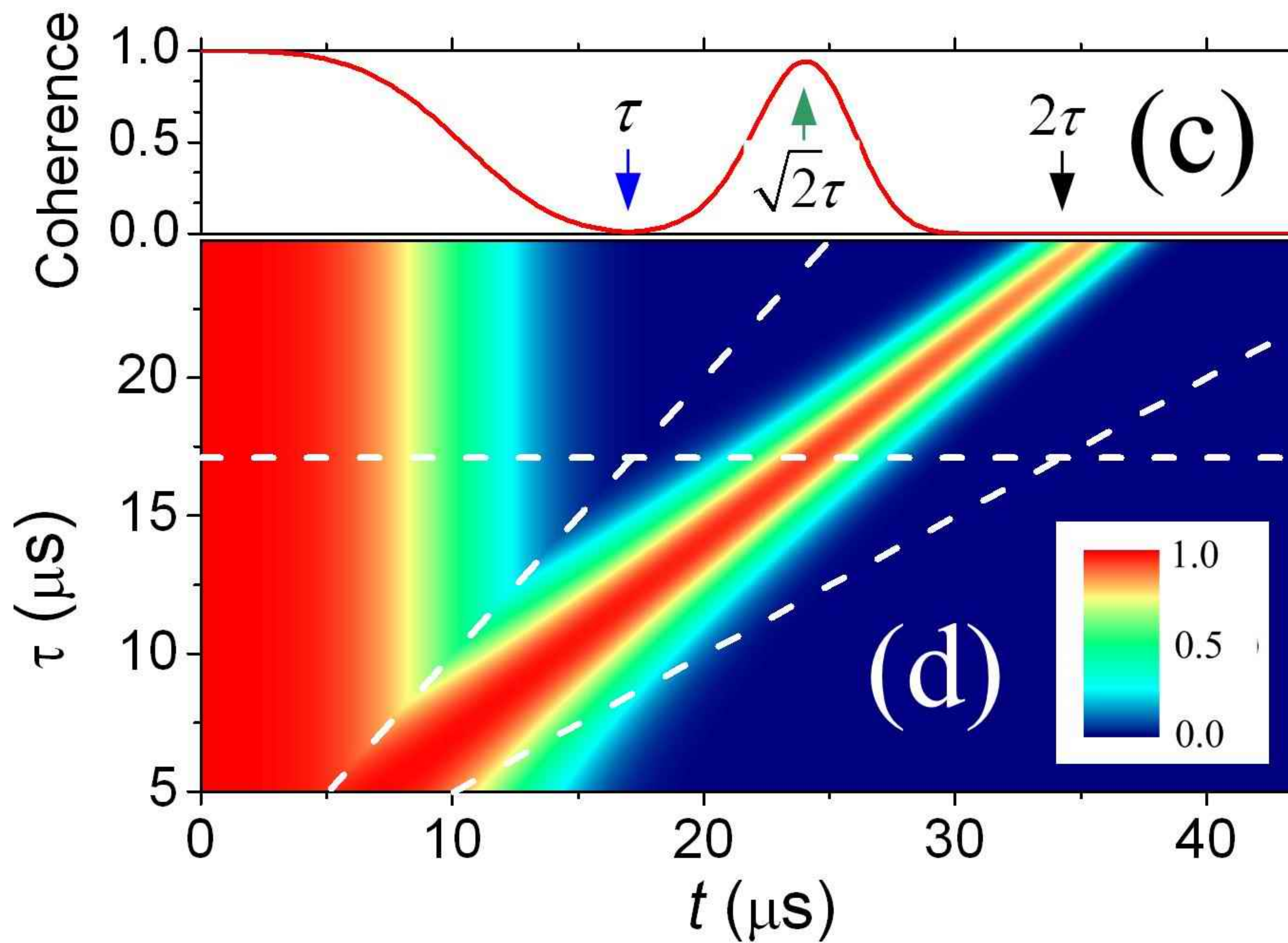
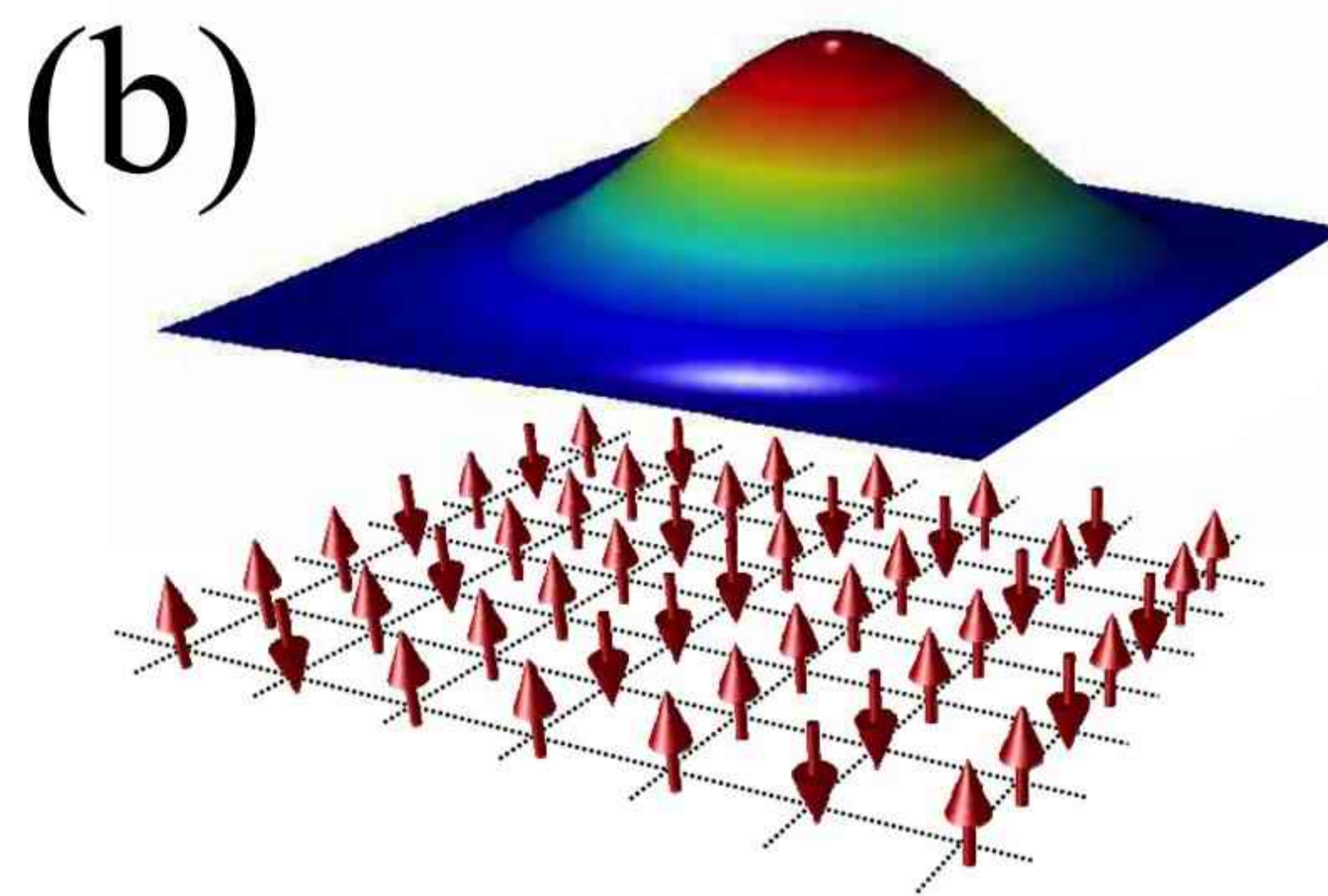
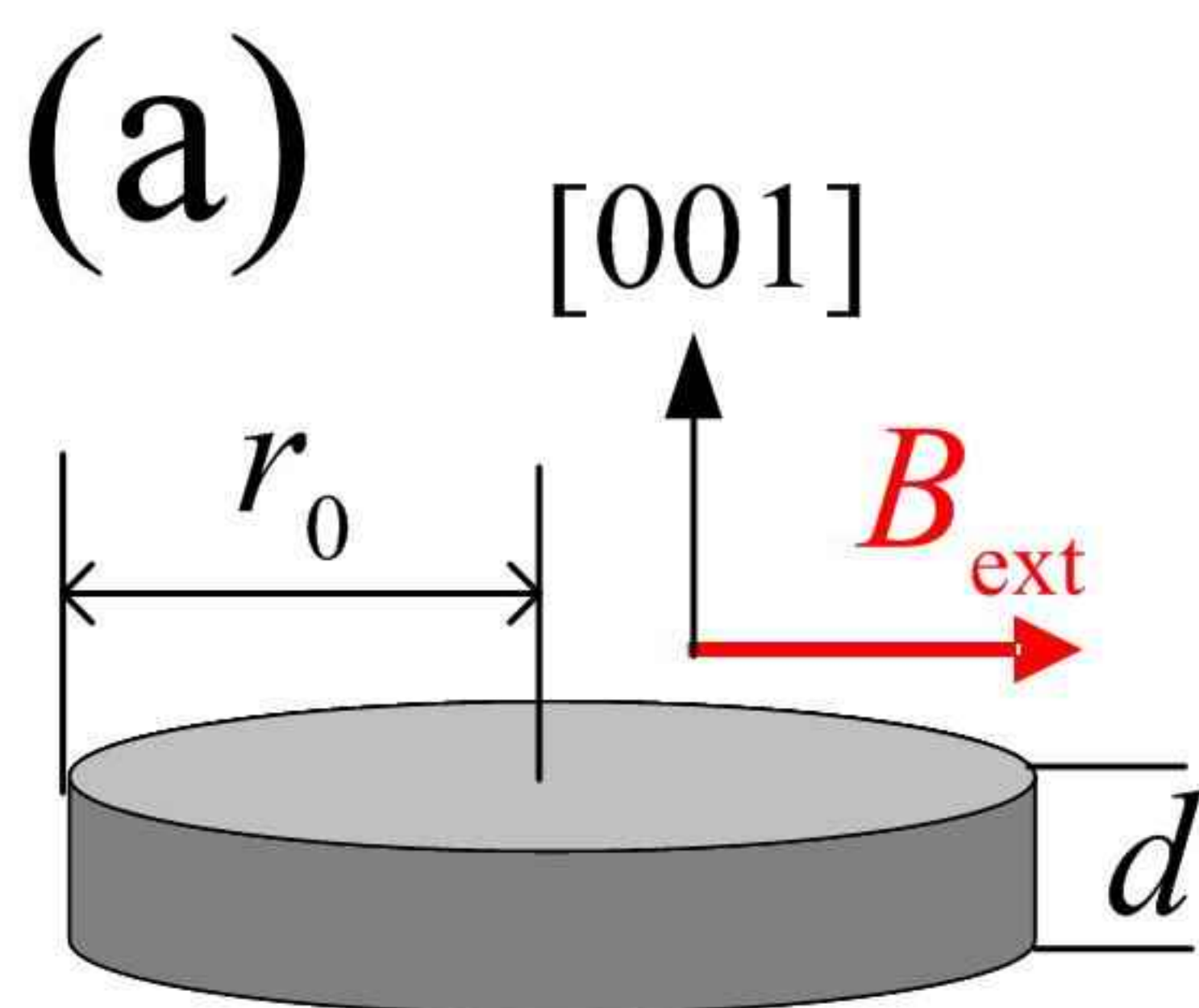
**Acknowledgements** We acknowledge support from NSF DMR-0403465, ARO/LPS, and DARPA/AFOSR

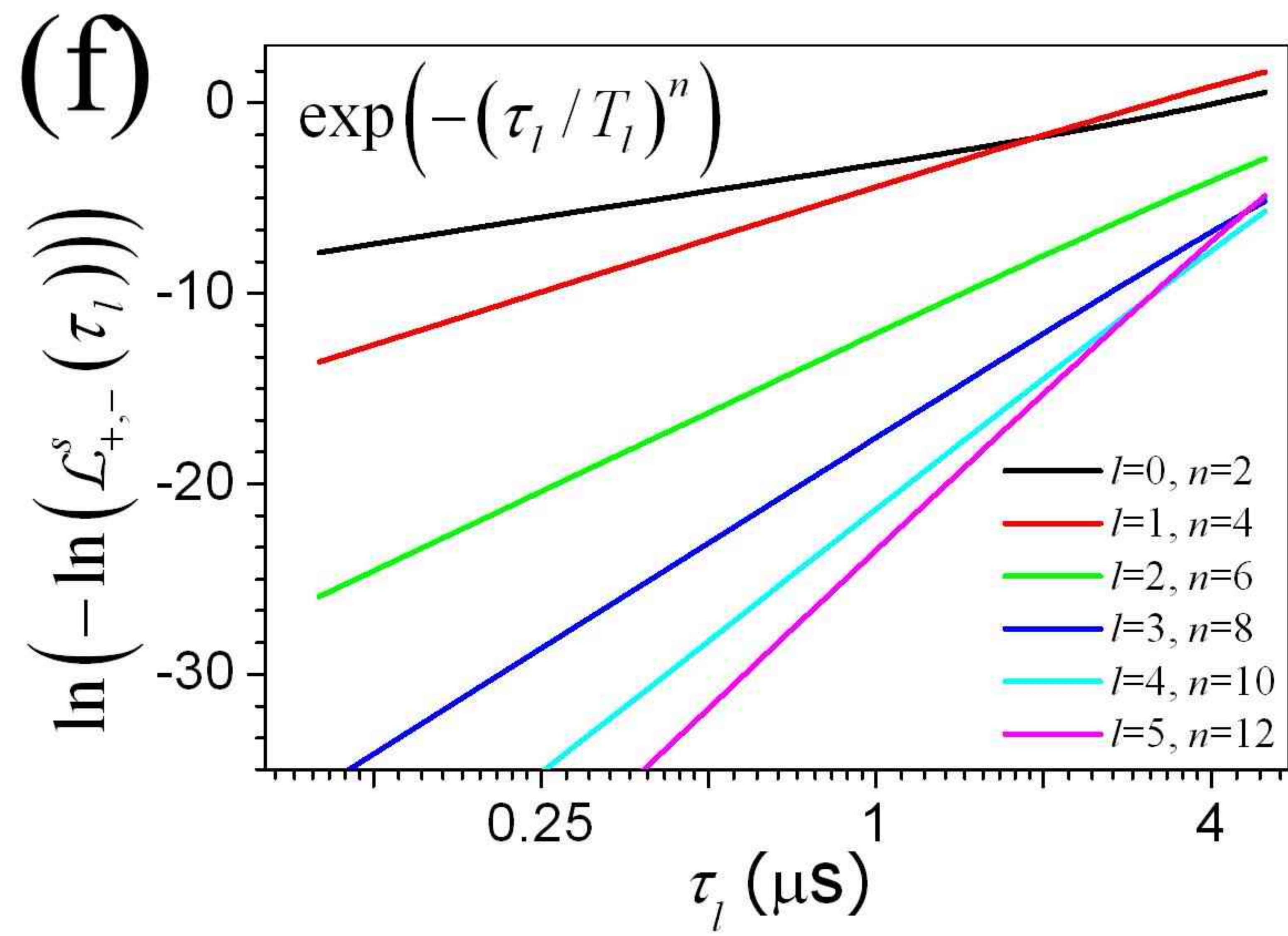
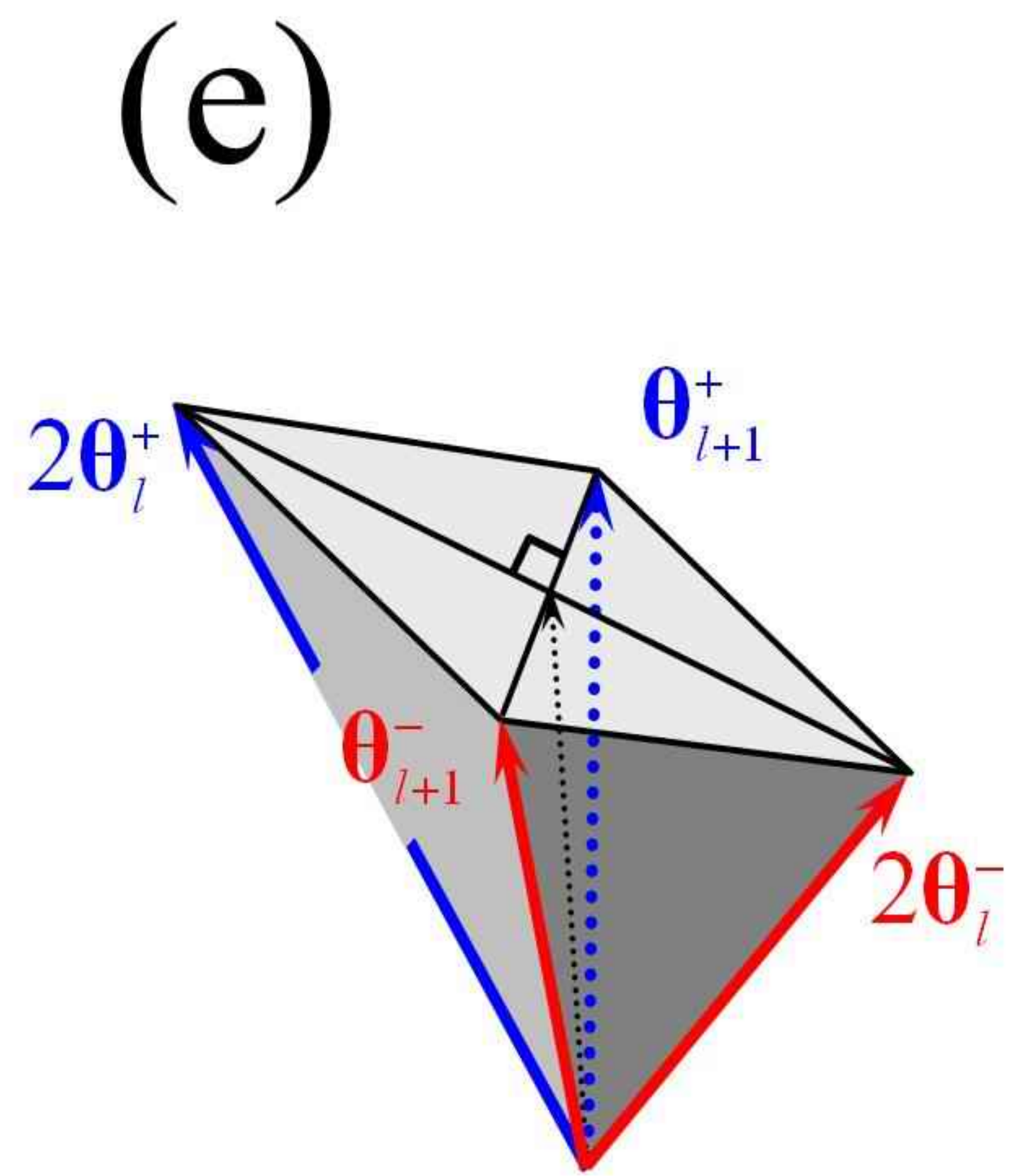
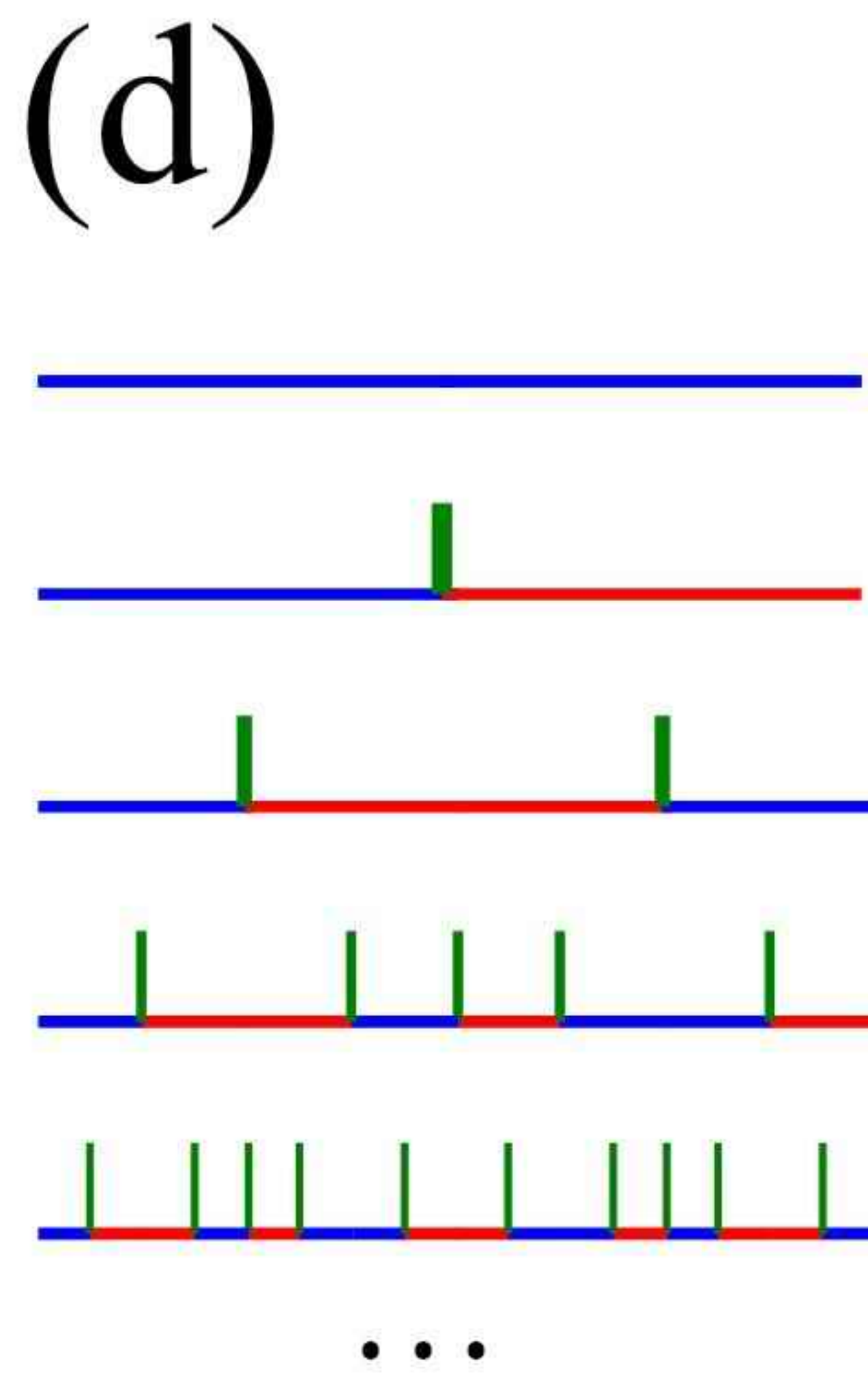
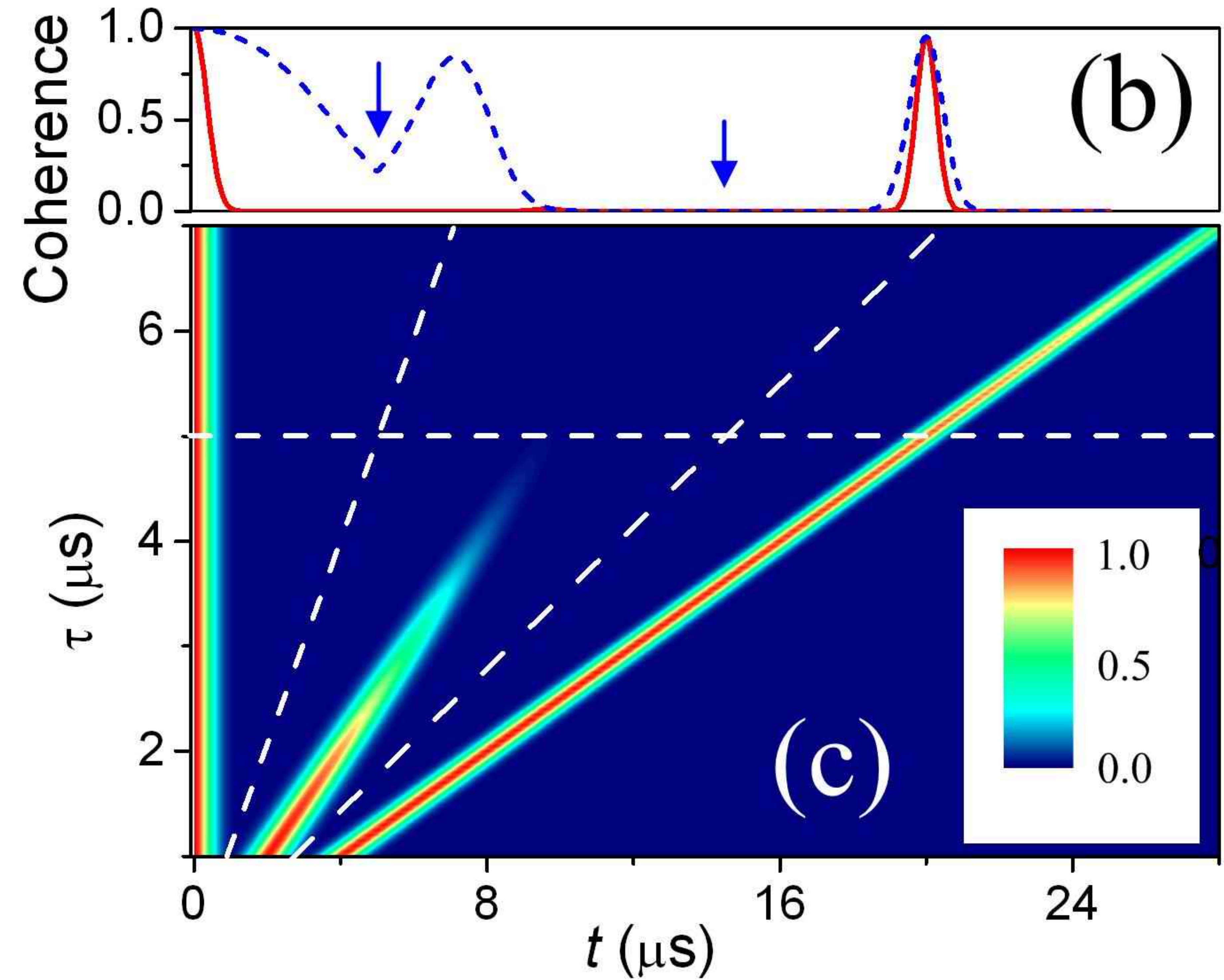
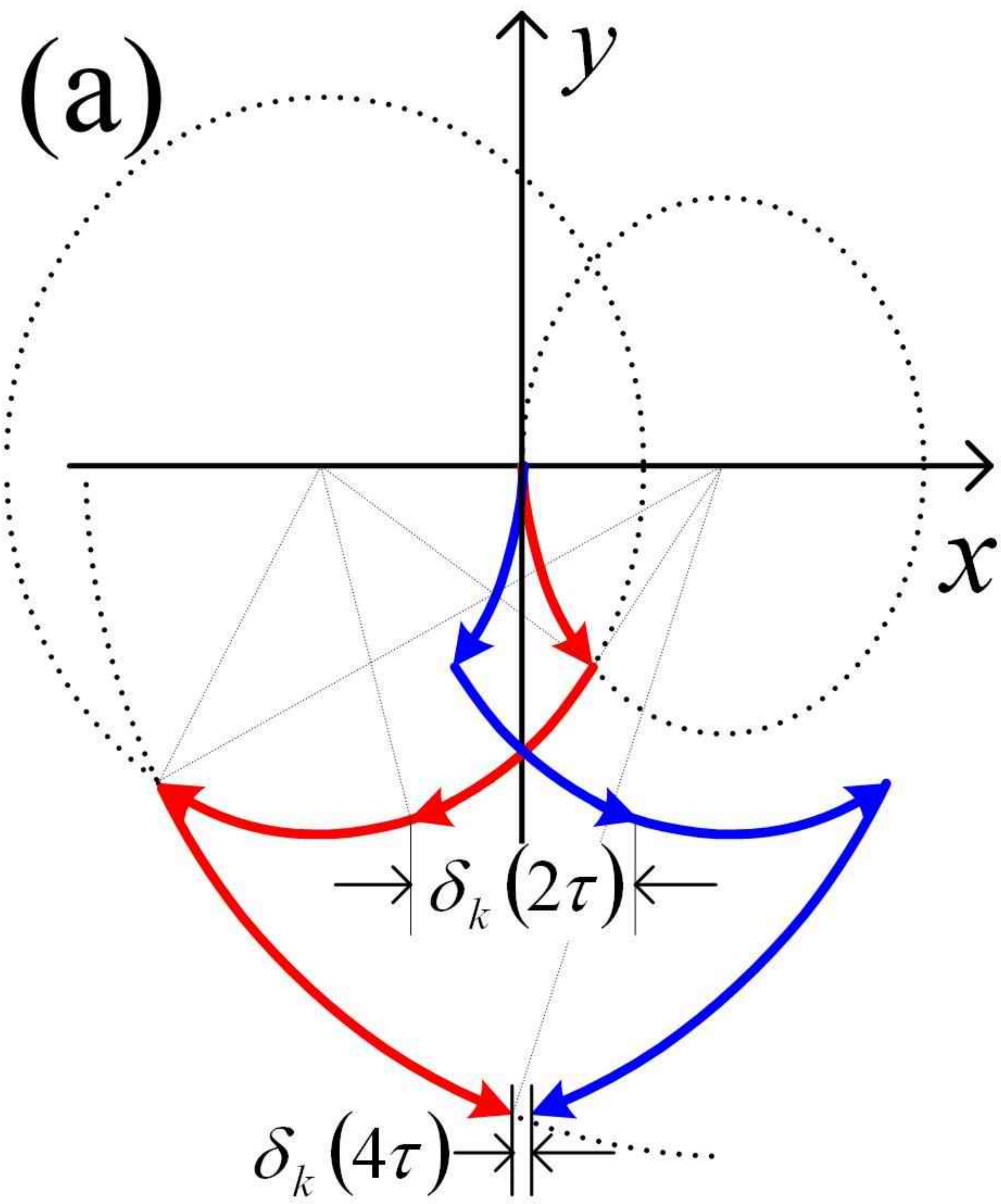
Fig. 1 (a) A GaAs quantum dot model with thickness  $d$  in growth direction [001] and lateral Fork-Darwin radius  $r_0$ , in an external magnetic field  $\mathbf{B}_{\text{ext}}$ . (b) Schematic illustration of an electron confined in the quantum dot containing many nuclear spins of a random configuration. The hyperfine interaction between the electron spin and the nuclear spins is determined by the electron's orbital wavefunction. (c) Electron spin coherence  $L_{+,-}^s(t)$  under the control of a single flip pulse applied at  $\tau = 17\mu\text{s}$  (indicated with the blue arrow). The lost coherence resurfaces and peaks at  $\sqrt{2}\tau$  (indicated with the green arrow) while coherence at conventional spin echo time  $2\tau$  (indicated with the black arrow) is vanishing. The entanglement induced decoherence time  $T_2 \sim 10\mu\text{s}$  can be inferred from the plot. (d) Contour plot of the electron spin coherence  $L_{+,-}^s(t)$  under the single pulse control as a function of the real time  $t$  and the pulse delay

time  $\tau$ . The pulse time  $\tau$  is indicated by the left tilted line. The restoration of the coherence is pronounced at  $\sqrt{2}\tau$  whereas no coherence peak is visible at the conventional echo time  $2\tau$  (indicated by the right tilted line). The horizontal line corresponds to the cut for the curve in (c). (e) The precession of the conjugated pseudo-spin Bloch vectors for local bath spin pairs under the single-pulse control. Red (blue) trajectory denotes the pseudo spin evolution  $|\psi_k^+\rangle$  ( $|\psi_k^-\rangle$ ). (f) The projection of Bloch vector trajectories to the  $x$ - $y$  plane. (g) Electron spin coherence  $L_{+-}^s(t)$  under the control by a sequence of  $\pi$ -rotations (indicated by blue vertical lines) evenly spaced by  $\tau = 10\mu\text{s}$ . The coherence peaks at every  $\sqrt{n(n+1)\tau}$  between the  $n$ th and the  $(n+1)$ th pulses. In the numerical evaluation, the dot size is given by  $d = 8.5$  nm and  $r_0 = 25$  nm, in the large- $N$  side of the mesoscopic regime, where the short-range direct nuclear interactions dominate<sup>16</sup>.  $\mathbf{B}_{\text{ext}} = 10$  T and is along the [110] direction. The electron spin  $g$ -factor is -0.44. The nuclear bath is initially in a product state  $|J\rangle \equiv \otimes_n |j_n\rangle$  randomly chosen from a thermal ensemble at temperature  $T=1$  K.

Fig. 2 (a) The pseudo-spin trajectories for local bath spin pairs under the control of two  $\pi$ -rotations applied on electron spin at  $\tau$  and  $3\tau$ . (b) The electron spin coherence under the two-pulse control with  $\tau = 5\mu\text{s}$ . The dashed blue line is the pure state dynamics part  $L_{+-}^s(t)$  and the solid red line is with the inhomogeneous broadening factor included  $L_{+-}^s(t) \times L_{+-}^0(t)$  (see text for explanation). The blue arrows indicate the time when the electron spin is flipped. (c) The contour plot of the ensemble-averaged electron spin coherence under the two-pulse control. The tilted dashed lines indicate the pulse times and the horizontal dashed line corresponds to the cut for the curve in (b). The coherence restoration related to the disentanglement is pronounced at the

second spin-echo time  $4\tau$  even when the first spin-echo at  $2\tau$  has been invisible. (d) Pulse sequences by concatenation design. The green spikes indicate the  $\pi$ -rotation pulses. Blue (red) horizontal lines denote the pseudo-spin evolution  $\hat{U}_0^\pm$  ( $\hat{U}_0^\mp$ ). The  $(l+1)$ th order sequence is constructed by two subsequent  $l$ th order sequences, with a pulse inserted if  $l$  is even. (e) Recursive relation between the vector rotation angles  $\theta_l^\pm$  for a pictorial understanding of the concatenation control (see Eqn. (7) in text). (f) The scaling of echo magnitude with the echo delay time  $\tau_l = 2^l \tau$  under the control of the concatenated pulse sequences in ensemble measurement. The quantum dot under consideration is of the same arrangement as in Fig. 1 but with  $d = 2.8$  nm and  $r_0 = 15$  nm. The nuclear bath is initially assumed in thermal equilibrium at  $T = 1$  k. In plot (b) and (c), we have artificially set the ensemble dephasing time  $T_2^*$  in  $L_{+-}^0(t)$  to  $0.5\mu s$ , about 100 times greater than its realistic value, to make the echo visible in the plot.





## Supplementary Information for “Restoring Coherence Lost to a Mesoscopic Bath”

Wang Yao, Ren-Bao Liu,\* and L. J. Sham

*Department of Physics, University of California San Diego,  
La Jolla, California 92093-0319, USA*

### Pseudo-spin model

We give the salient points of the method of solving the electron nuclear spin dynamics in a GaAs quantum dot. The system consists of an electron with spin vector  $\hat{\mathbf{S}}_e$  and  $N$  nuclear spins,  $\hat{\mathbf{J}}_n$ , with Zeeman energies  $\Omega$  and  $\omega_n$  under a magnetic field  $B_{\text{ext}}$ , respectively, where  $n$  denotes both positions and isotope types ( $^{75}\text{As}$ ,  $^{69}\text{Ga}$  and  $^{71}\text{Ga}$ ). The interaction can be separated as “diagonal” (or “longitudinal”) terms which involve only the spin vector components along the field ( $z$ ) direction and “off-diagonal” (or “transverse”) terms which involve spin flips. Because  $\Omega$  is much larger than  $\omega_n$  and the strength of the direct nuclear-nuclear interactions (e.g., nuclear dipolar interaction), the off-diagonal part of the electron nuclear hyperfine interaction can be eliminated by a standard canonical transformation, with the second-order correction left as the hyperfine-mediated nuclear-nuclear interaction. For the same reason, the off-diagonal part of the nuclear-nuclear interaction includes only terms which conserve the Zeeman energies, thus excluding the hetero-nuclear terms. The total effective Hamiltonian can be written as  $\hat{H} = \hat{H}_e + \hat{H}_N + \sum_{\pm} |\pm\rangle \hat{H}^{\pm} \langle \pm|$ , with  $\hat{H}_e = \Omega \hat{S}_e^z$ ,

---

\*Present address: Department of Physics, The Chinese University of Hong Kong, Hong Kong, China

$\hat{H}_N = \omega_n \hat{J}_n^z$ ,  $\hat{H}^\pm = \pm \hat{H}_A + \hat{H}_B + \hat{H}_D \pm \hat{H}_E$ , and

$$\hat{H}_A = \sum_{n \neq m}' \frac{a_n a_m}{4\Omega} \hat{J}_n^+ \hat{J}_m^- \equiv \sum_{n \neq m}' A_{n,m} \hat{J}_n^+ \hat{J}_m^-, \quad (1a)$$

$$\hat{H}_B = \sum_{n \neq m}' B_{n,m} \hat{J}_n^+ \hat{J}_m^- \quad (1b)$$

$$\hat{H}_D = \sum_{n < m} D_{n,m} \hat{J}_n^z \hat{J}_m^z \quad (1c)$$

$$\hat{H}_E = \sum_n (a_n/2) \hat{J}_n^z \equiv \sum_n E_n \hat{J}_n^z, \quad (1d)$$

where  $|\pm\rangle$  are the eigenstates of  $\hat{S}_e^z$ , the summation with a prime runs over only the homonuclear pairs, the subscript  $A$  denotes the hyperfine mediated nuclear-nuclear interaction,  $B$  the off-diagonal part of the direct nuclear-nuclear interaction,  $D$  the diagonal part of the direct nuclear-nuclear interaction, and  $E$  the diagonal part of the contact electron-nuclear hyperfine interaction. The hyperfine energy, determined by the electron orbital wavefunction, has a typical energy scale  $E_n \sim a_n \sim \frac{\mathcal{A}}{N} \sim 10^6 \text{ s}^{-1}$  for a dot with about  $10^6$  nuclei [1], where  $\mathcal{A}$  is the hyperfine constant depending only on the element type. The direct nuclear-nuclear interaction, which is “short-ranged” (referred here as decaying no slower than dipolar), has the near-neighbor coupling  $B_{n,m} \sim D_{n,m} \sim b \sim 10^2 \text{ s}^{-1}$ . The hyperfine mediated interaction, which couples any two nuclear spins that are in contact with the electron and is associated with opposite signs for opposite electron spin states, has an energy scale dependent on the field strength,  $A_{n,m} \sim \frac{\mathcal{A}^2}{N^2 \Omega} 1\text{--}10 \text{ s}^{-1}$  for field  $\sim 40\text{--}1 \text{ T}$ . This hyperfine mediate interaction is differentiated from the “short-range” direct nuclear-nuclear interaction by the qualifier “infinite-range”. We work in the interaction picture defined by  $\hat{H}_e$  and  $\hat{H}_N$  in which the dynamics are determined by  $\hat{H}^\pm$ .

The basis set of the bath are eigenstates of  $\hat{H}_N$ :  $\bigotimes_n |j_n\rangle$ . In Eqn. (1),  $\hat{H}_D$  and  $\hat{H}_E$  are diagonal in this basis. The off-diagonal terms  $\hat{H}_A$ ,  $\hat{H}_B$  are weak perturbations that will excite the bath initially on an arbitrary configuration  $|J\rangle \equiv |j_1\rangle \cdots |j_N\rangle$ . The elementary excitations in the nuclear spin bath are pair-flip excitations created by operators  $\hat{J}_m^+ \hat{J}_n^-$  in the reduced Hamiltonian. Starting from any initial nuclear configuration, the evolution of the nuclear spin states by these elementary excitations is of the hierarchy as shown in the left side of Fig. 1. We can regard the zeroth layer of this hierarchy, the initial state, as the ‘vacuum’ of the pair-flip excitations and layer  $n$  corresponds to  $n$  pair-flip excitations have

been created. The state at time  $t$  is a linear superposition of all possibilities:

$$|J(t)\rangle = C_J(t)|J\rangle + \sum_{m,n} C_{m,n}(t)\hat{J}_m^+\hat{J}_n^-|J\rangle + \sum_{l,p,m,n} C_{l,p,m,n}(t)\hat{J}_l^+\hat{J}_p^-\hat{J}_m^+\hat{J}_n^-|J\rangle + \dots \quad (2)$$

where the summation over the indexes  $m, n, l, p, \dots$  are defined such that  $|J\rangle$ ,  $\hat{J}_m^+\hat{J}_n^-|J\rangle$ ,  $\hat{J}_l^+\hat{J}_p^-\hat{J}_m^+\hat{J}_n^-|J\rangle, \dots$  denote different eigenstates of  $\hat{H}_N$  orthogonal to each other.

We solve this dynamics in the nuclear spin bath based on a pseudo-spin model as described below. We have, on sites labelled  $n = 1, \dots, N$ , the nuclear spin states  $|j_n\rangle$  with  $-j \leq j_n \leq j$  for nuclei of spin  $j$ . As the elementary excitations are pair dynamics driven by  $\hat{J}_m^+\hat{J}_n^-$ , we first sort out the pair states  $|j_n\rangle|j_m\rangle$ . These pair states are divided into three categories:

1. *Down States*: A down state  $|j_n\rangle|j_m\rangle$  has a partner  $|j_n + 1\rangle|j_m - 1\rangle$  created by

$$\hat{J}_n^+\hat{J}_m^-|j_n\rangle|j_m\rangle = \sqrt{(j + j_n + 1)(j - j_n)}\sqrt{(j - j_m + 1)(j + j_m)}|j_n + 1\rangle|j_m - 1\rangle$$

A down state must have  $(j_n < j, j_m > -j)$ . There are  $(2j)^2$  down states for each bond.

2. *Up States*: An up state  $|j_n\rangle|j_m\rangle$  has a partner  $|j_n - 1\rangle|j_m + 1\rangle$  created by  $\hat{J}_n^-\hat{J}_m^+|j_n\rangle|j_m\rangle$ .

The up state must have  $(j_n > -j, j_m < j)$ . There are  $(2j)^2$  up states for each bond.

3. *Single States*: A single pair state has no partners connected by  $\hat{J}_n^-\hat{J}_m^+|j_n\rangle|j_m\rangle$  or its Hermitian conjugate, i.e.,  $j_n = j_m = j$  or  $j_n = j_m = -j$ .

The single states may be mapped to pseudo-spin 0 states. Since they are scalar states, their Hamiltonian terms will commute with every other operators, they can only contribute to the phase factor in the electron spin coherence through the Overhauser field, causing inhomogeneous broadening.

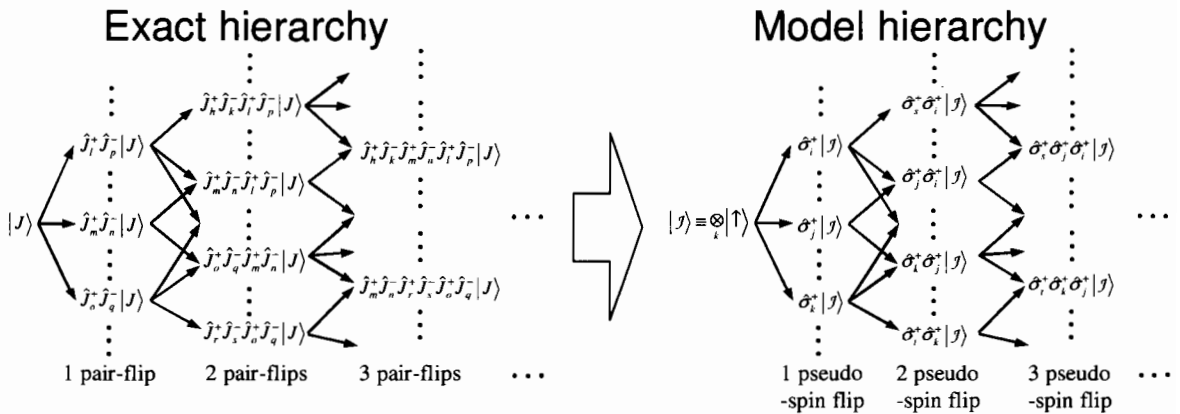


FIG. 1: Hierarchy of the nuclear spin dynamics.

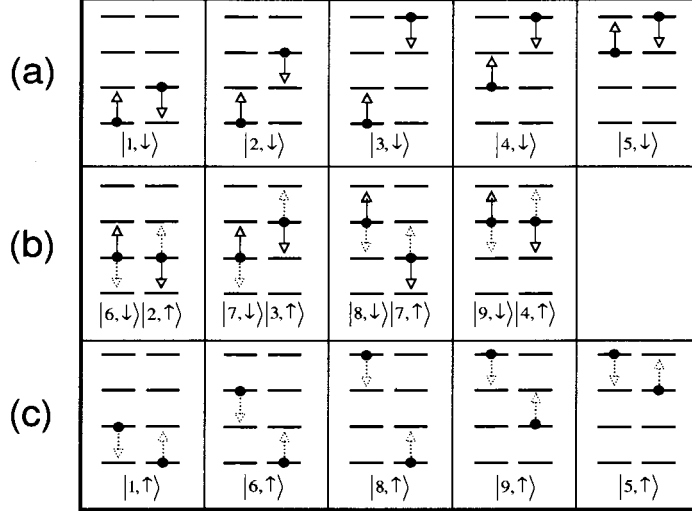


FIG. 2: Illustration of mapping from pair states to pseudo-spin states for nuclei of spin 3/2. The solid dots show state  $|j_m\rangle|j_n\rangle$ . The state vector show the mapped state  $|k,\sigma\rangle$ . The solid arrows between lines show to which state the operator  $\hat{J}_m^+ \hat{J}_n^-$  would lead and the dotted arrows show to which state  $\hat{J}_m^- \hat{J}_n^+$  would lead. (a) Monogamy states with pseudo-spin down. (b) Bigamy states which are mapped to two pseudo-spins with one up and one down respectively. (c) Monogamy states with pseudo-spins up.

We shall find by an explicit construction that the up and down states can be paired to provide states of  $(2j)^2$  two-level systems - the pseudo-spins. These states are divided into:

1. *Monogamy States*: Each state belongs to only one pseudo-spin although its partner may be a bigamist. These states are edge states in that at least one of the two spin quantum numbers ( $j_n$  or  $j_m$ ) equal to  $\pm j$  but they cannot both be equal to  $j$  or to  $-j$ . Half of them ( $4j - 1$  states) are down states,  $|j_n = -j\rangle|j_m > -j\rangle$  or  $|j_n < j\rangle|j_m = j\rangle$ , see Fig. 2(a). The other  $4j - 1$  states,  $|j_n > -j\rangle|j_m = -j\rangle$  or  $|j_n = j\rangle|j_m < j\rangle$  are up states, see Fig. 2(c).

2. *Bigamy States*: Each belongs to two different pseudo-spins. They are interior states:  $-j < j_n < j$  and  $-j < j_m < j$ . There are  $(2j - 1)^2$  of them, see Fig. 2(b).

The mapping to pseudo-spins is carried out by labelling the set of down monogamy and bigamy states,  $p(j_n, j_m) = 1, \dots, (2j)^2$ . Note that  $p$  depends only on the spin quantum numbers. The state mapping for the down states is,

$$|j_n\rangle|j_m\rangle \rightarrow |p(j_n, j_m) \downarrow\rangle.$$

Next, we match from each  $|j_n\rangle|j_m\rangle$  of the above set, the partner state  $|j_n+1\rangle|j_m-1\rangle$ , which will be a member of either the up monogamy or bigamy set. Thus,

$$|j_n+1\rangle|j_m-1\rangle \rightarrow |p(j_n, j_m) \uparrow\rangle.$$

These two steps are illustrated for  $j = 3/2$  in Fig. 2. Notice that by the above mapping to the pseudo-spins, each bigamy state has been mapped to the product of an up state of one pseudo-spin and a down state of another,

$$|j_n\rangle|j_m\rangle \rightarrow |p(j_n, j_m) \uparrow\rangle \otimes |p'(j_n, j_m) \downarrow\rangle.$$

as shown in Fig. 2(b)

For any initial configuration  $|J\rangle$ , the relevant set of pseudo-spins  $\mathcal{G}_J$  is determined by examining every possible nuclear spin pair  $(m, n)$ . Each pair will contribute 0, 1 or 2 pseudo-spins if  $|j_m\rangle|j_n\rangle$  is in the single state, Monogamy state or Bigamy state configuration respectively (see Fig. 2). The many nuclear spin initial state  $|J\rangle$  is then mapped to,

$$|J\rangle \equiv |j_1\rangle \cdots |j_N\rangle \Rightarrow |\mathcal{J}\rangle \equiv \bigotimes_{k \in \mathcal{G}_J} |k\sigma\rangle \quad (3)$$

where  $k$  labels both the nuclear pair  $(m, n)$  and the pseudo-spin type  $p(j_n, j_m)$ .  $\sigma = \uparrow$  or  $\downarrow$  depending on whether  $k$  is mapped from up or down Monogamy or Bigamy state. Different initial nuclear configurations will result in different sets of pseudo-spins. For a randomly chosen initial configuration  $|J\rangle$ , the number of pseudo-spins is given by  $M \sim (\frac{2j}{2j+1})^2 ZN$  where  $N$  is the total number of nuclear spins and  $Z$  the number of nuclei coupled to a particular nuclear spin by the nuclear-nuclear interaction. For short ranged direct interaction,  $Z \sim O(10)$  and for the infinite-ranged hyperfine mediated interaction  $Z = N$ . The factor  $(\frac{2j}{2j+1})^2$  arises as the single state, Monogamy state and Bigamy state are contributing 0, 1 and 2 pseudo-spins respectively. For convenience, when the set  $\mathcal{G}_J$  is determined from the  $|J\rangle$ , we redefine the pseudo-spin up and down states, i.e.  $|k, \sigma\rangle \rightarrow |k, -\sigma\rangle$ , for those pseudo-spins in set  $\mathcal{G}_J$  so that the initial state  $|\mathcal{J}\rangle$  in this new definition corresponds to all pseudo-spins pointing ‘up’:  $\bigotimes_k |\uparrow\rangle_k$ . The redefinition is conditioned on the initial nuclear configuration  $|J\rangle$ .

The original Hamiltonian  $\hat{H}^\pm$  is mapped to the pseudo-spin Hamiltonian of the form,

$$\hat{H}_{\text{sp}}^\pm = \sum_k \hat{\mathcal{H}}_k^\pm \equiv \sum_k \mathbf{h}_k^\pm \cdot \hat{\boldsymbol{\sigma}}_k / 2 \quad (4)$$

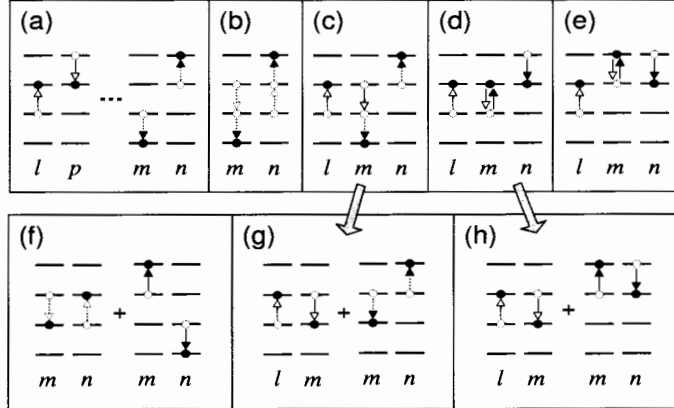


FIG. 3: Illustration of multi pair-flip excitations in the nuclear bath. We use hollow arrowheads to indicate the first pair-flip and solid arrowheads to indicate the second pair-flip. Dotted arrows denote the pseudo-spin flip from 'down' state to 'up' state and solid arrows for the inverse process (see text). (a) Independent pair flips; (b-e) Various situations of overlapping pair-flips; (f-h) Approximations in the independent pseudo-spin model.

The effective magnetic field  $\mathbf{h}_k^\pm$  on the pseudo-spins, conditioned on the electron spin state, are to be determined by reproducing the matrix elements,  $\langle J | \hat{J}_m^+ \hat{J}_n^- \hat{H}^\pm \hat{J}_n^+ \hat{J}_m^- | J \rangle - \langle J | \hat{H}^\pm | J \rangle$  and  $\langle J | \hat{H}^\pm \hat{J}_n^+ \hat{J}_m^- | J \rangle$ , namely the energy cost and transition matrix element for nuclear pair-flips.

The pseudo-spin model for characterizing the nuclear spin bath dynamics is to approximate the exact evolution of Eqn. (2) by the independent evolution of all pseudo-spins in  $\mathcal{G}_J$ ,

$$|\mathcal{J}(t)\rangle = \bigotimes_{k \in \mathcal{G}_J} |\psi_k^\pm(t)\rangle = C_{\mathcal{J}}(t)|\mathcal{J}\rangle + \sum_{k_1} C_{k_1}(t) \hat{\sigma}_{k_1}^+ |\mathcal{J}\rangle + \sum_{k_1, k_2} C_{k_1, k_2}(t) \hat{\sigma}_{k_1}^+ \hat{\sigma}_{k_2}^+ |\mathcal{J}\rangle + \dots \quad (5)$$

This pseudo-spin dynamics can be put into a similar hierarchy as shown in the right part of Fig. 1 which we will refer to as model hierarchy in contrast to the exact hierarchy.

With the mapping established for the state (Eqn. (3)) and the Hamiltonian (Eqn. (4)), the first two layers of the exact hierarchy will be reproduced exactly by the model hierarchy, i.e., there is a one to one correspondence between  $\hat{J}_m^+ \hat{J}_n^- | J \rangle$  and  $\hat{\sigma}_k^+ |\mathcal{J}\rangle$  with the energy and coupling to the initial state  $| J \rangle$  ( $|\mathcal{J}\rangle$ ) exactly reproduced.

Difference between the model and the exact hierarchies arises when more than one excitations have been created in the system. In Fig. 3, we illustrate with the case when two pair-flip

excitations have been created. If the two pair-flips do not overlap as shown in Fig. 3(a), their dynamics are then independent of each other and well described by the pseudo-spin model. Fig.3(b-e) illustrate the various situations that the two pair-flips overlap, by sharing one or two nuclei. The flip-flop of the first nuclear pair  $(l, m)$  changes the spin configuration of both nuclear  $l$  and  $m$  and if a second flip-flop is to take place on pair  $(l, m)$  or  $(n, m)$  or  $(l, n)$ , it is no longer described by the dynamics of the original pseudo-spins assigned to it. Instead, in the model hierarchy by the independent pseudo-spin model, two successive flip-flops on pair  $(l, m)$  or two successive flip-flops on pair  $(l, m)$  and  $(m, n)$  respectively are shown in Fig.3(f-h). Fig. 3(g) can be considered as the approximate form of Fig. 3(c) and Fig. 3(h) as that of Fig. 3(d). The model hierarchy contains events like Fig. 3(f) which is absent in the exact hierarchy and events like Fig. 3(e) in the exact hierarchy is not contained in the model hierarchy. Therefore, on layer 2, the model hierarchy coincides with the exact hierarchy in events described by Fig. 3(a) and differ by replacing the events of Fig.3(b-e) with events of Fig.3(f-h). The difference in a general layer can be analyzed in the same way.

By the pseudo-spin model, we are using Eqn. (5) as the bath state at time  $t$  for calculating physical properties instead of Eqn. (2). The difference of the exact and model hierarchies is estimated below which serves as an upper bound for error estimation (notice that the physical properties of interest are not necessarily changed by replacing events of Fig.3(b-e) with events of Fig.3(f-h), therefore, this error-estimation is not necessarily a tight bound). If  $n - 1$  pair-flip excitations have already been generated, to create the next excitation, we have  $M$  pseudo-spin to choose from and  $\sim 2(n - 1)Z$  of them overlap with the previous excitations. Therefore, the probability of having a new excitation without overlapping with the previous excitations is given by:  $\sim \frac{M - 2(n - 1)Z}{M}$ . By induction, the probability of creating  $n$  non-overlapping pair-flip excitations is then given by,

$$\begin{aligned} p(n) &\simeq 1 \times \frac{M - 2Z}{M} \times \frac{M - 2(n - 1)Z}{M} \dots \times \frac{M - 2(n - 1)Z}{M} \\ &\simeq \exp \left[ -\frac{2Z}{M} - \dots - \frac{2(n - 1)Z}{M} \right] \\ &= \exp \left[ -\frac{n(n - 1)}{N} \left( \frac{2j + 1}{2j} \right)^2 \right] \end{aligned} \quad (6)$$

The second  $\simeq$  holds if  $2nZ \ll M$  which is always true in the timescale relevant in our study.

Comparing the model hierarchy and the exact hierarchy, we find from the above analysis that they differ in layer  $n$  with the relative amount of  $1 - p(n)$ .

### Error estimation

We perform a self-consistent analysis on validity of the pseudo-spin model. Here the relevant timescale plays the crucial role in determine the validity of the model. If only the first  $n$  layers of the hierarchy (the exact one and the model one) are involved, the error in the calculated physical properties is bounded by  $1 - p(n) \ll 1$  if  $n^2 \ll N$ . Therefore, in the very short time limit, only the first several layers of the hierarchy can be involved and the pseudo-spin model gives an almost exact account of the dynamics. To estimate error upper bound for the longer time limit, we will calculate the number of layers involved (denoted as  $n$ ) based on the model hierarchy of the pseudo-spin model. If  $n^2/N$  obtained is small, we conclude that  $n$  also faithfully reflects the number of layers involved in the exact hierarchy. Therefore, the error estimation based on the pseudo-spin model is faithful and any physical properties calculated based on pseudo-spin model is also a good approximation since the difference from the exact dynamics is small. Otherwise, the approximation is not good. It is established below that the condition  $n^2 \ll N$  is the origin of an upper bound and a lower bound on the quantum dot size  $N$  for which our theory is able to deal with. The validity of the pair-correlation approach (pseudo-spin model) is indeed in the mesoscopic regime.

At any given time  $t$ , an average excitation number  $N_{flip}(t)$  can be defined as follows based on the model hierarchy,

$$N_{flip}(t) = 1 \times \sum_{k_1} |C_{k_1}(t)|^2 + 2 \times \sum_{k_1, k_2} |C_{k_1, k_2}(t)|^2 + 3 \times \sum_{k_1, k_2, k_3} (t) |C_{k_1, k_2, k_3}|^2 + \dots \quad (7)$$

and our analysis [2] shows that the layer-distribution of population in the hierarchy is of a normal distribution centered at  $N_{flip}$ , i.e. the population is distributed in layers from layer  $N_{flip} - \sqrt{N_{flip}}$  to  $N_{flip} + \sqrt{N_{flip}}$ . Therefore, the quantity for characterizing the error upper bound is of a very simple form:  $P_{err}(t) \equiv 1 - \exp(-N_{flip}^2(t)/N)$ .

In the pseudo-spin model,  $N_{flip}(t)$  defined in Eqn. (7) has an equivalent expression which is more convenient for evaluation:

$$N_{flip}(t) = \sum_k |\langle \downarrow |U_k^\pm(t)| \uparrow \rangle|^2 \quad (8)$$

where  $U_k^\pm(t) \equiv e^{-i\hat{\mathcal{H}}_k^\pm t}$  is the evolution operator for pseudo-spin  $k$ . The contribution can be divide into two parts:  $N_{flip}(t) = N_{flip}^A(t) + N_{flip}^B(t)$ .  $N_{flip}^A$  is the number of non-local pair-flip excitations and  $N_{flip}^B$  is the number of local pair-flip excitations that have been created.

$N_{flip}^A(t)$  and  $N_{flip}^B(t)$  have very different behavior and we analyze them separately.

In free-induction evolution, the number of non-local pair-flip excitations is given by,

$$N_{flip}^A(t) = \sum_k \left( \frac{2A_k}{h_k^A} \right)^2 \sin^2 \frac{h_k^A t}{2} \leq \sum_k A_k^2 t^2 \simeq M_A \frac{\mathcal{A}^4}{N^4 \Omega^2} t^2 \simeq \frac{\mathcal{A}^4}{N^2 \Omega^2} t^2$$

where  $h_k^A \equiv \sqrt{E_k^2 + 4A_k^2}$  and  $M_A \sim N^2$  is the number of non-local nuclear spin pairs. Since the evolution of the non-local pair-correlation is completely reversed by the  $\pi$  pulses,  $N_{flip}^A(t)$  is also reversed and  $N_{flip}^A = 0$  at each spin echo time. Therefore,  $N_{flip}^A(t)$  does not accumulate in the pulse controlled dynamics and we just need to look at the maximum value of  $N_{flip}^A(t)$  between echoes. For example, in the control with the equally spaced pulse sequence, in order to have the coherence well preserved or restored at spin echo time, the delay time between successive pulses is limited by  $\tau \lesssim T_H$ , where  $T_H \simeq b^{-1/2} \mathcal{A}^{-1/2} N^{1/4}$  is the Hahn echo decay timescale and  $\sim 10\mu\text{s}$  in GaAs [3]. Therefore,  $N_{flip}^A$  at any time is bounded by  $N_{flip}^A(\mathcal{O}(T_H))$  in this scenario. The estimate of the bound on  $N$  imposed by  $N_{flip}^A$  for the validity of our approach is therefore,

$$\left( \frac{\mathcal{A}^4}{N^2 \Omega^2} T_H^2 \right)^2 \frac{1}{N} \sim \frac{\mathcal{A}^6}{N^4 \Omega^4 b^2} \ll 1 \quad (9)$$

For GaAs fluctuation dot in a magnetic field of 10 Tesla, the above condition is well satisfied for  $N \gtrsim 10^4$ . Estimation for other controlling pulse sequences give a lower bound on  $N$  which is in the same order.

For the number of local pair-flip excitations, we have a similar expression in the free-induction evolution,

$$N_{flip}^B(t) = \sum_k \left( \frac{2B_k}{h_k^B} \right)^2 \sin^2 \frac{h_k^B t}{2} \leq \sum_k B_k^2 t^2 \simeq M_B b^2 t^2 \simeq \alpha N b^2 t^2$$

where  $h_k^B \equiv \sqrt{E_k^2 + 4B_k^2}$  and  $M_B \sim \alpha N$  is the number of local nuclear spin pairs.  $\alpha$  ( $\sim 10$  in GaAs) is determined by number of local neighbors and the nuclear spin quantum number  $j$ . In contrast to the non-local pair dynamics, the local pair dynamics is *not* reversed under the influence of the electron spin flip and  $N_{flip}^B(t)$  accumulates all through the time. Nonetheless, it turns out that  $N_{flip}^B(t) \leq \sum_k B_k^2 t^2 \simeq \alpha N b^2 t^2$  holds for all scenarios of pulse controls being discussed. Therefore, the condition  $(N_{flip}^B)^2/N \ll 1$  sets an upper bound on  $N$ :  $N \alpha^2 (bt)^4 \ll 1$ , which depends on the time range  $t$  we wish to explore. Alternatively speaking,  $(N_{flip}^B)^2/N \ll 1$  sets an upper bound on the time range  $t$  we can explore for some

fixed  $N$  using the pseudo-spin model. We illustrate this bound using the following two examples.

1. If we wish to calculate the Hahn echo signal using the pseudo-spin model, we shall have  $(\alpha Nb^2 T_H^2)^2/N \ll 1$  where the Hahn echo decay time  $T_H \approx b^{-1/2} \mathcal{A}^{-1/2} N^{1/4}$  [3]. Therefore, the upper bound on  $N$  is given by  $N^2 \alpha^2 b^2 \mathcal{A}^{-2} \ll 1$ . For GaAs quantum dot, this condition is well satisfied for  $N \lesssim 10^8$ .
2. For bath of an intermediate size in the allowed region of  $\min[\sqrt{N}, N^4 b^2 \Omega^4 \mathcal{A}^{-6}] \gg 1 \gg \alpha^2 N^2 b^2 \mathcal{A}^{-2}$ , e.g., a quantum dot of typical size  $N \sim 10^5 - 10^6$  in our problem,  $(\alpha Nb^2 t^2)^2/N \ll 1$  is satisfied for a much longer time range  $t \sim 10T_H \sim 100\mu s$ .

In summary, for the pair-correlation approximation (or pseudo-spin model) to be valid, nuclear spin dynamics of local pair-flips imposes an upper bound on  $N$  while nuclear spin dynamics of non-local pair-flips imposes a lower bound. Within this mesoscopic regime, the pair-correlation approximation is well justified. The error estimation is based on characterizing the difference in the Hilbert space structure of the exact dynamics and that of the pseudo-spin model and assuming this difference has a full influence on the electron spin coherence calculation. Therefore, the bound is not necessarily tight and it is possible that the pulse control methodology developed using the pseudo-spin model have actually a much larger validity regime. Investigation is underway.

---

[1] D. Paget, G. Lampel, and B. Sapoval, Phys. Rev. B **15**, 5780 (1977).  
[2] W. Yao, R. B. Liu, and L. J. Sham, unpublished data.  
[3] W. Yao, R. B. Liu, and L. J. Sham, cond-mat/0508441 (2005).